Neuroscience 286 (2015) 122–130

REDUCED PHOSPHORYLATION OF SYNAPSIN I IN THE HIPPOCAMPUS OF ENGRAILED-2 KNOCKOUT MICE, A MODEL FOR AUTISM SPECTRUM DISORDERS

G. PROVENZANO,[a†] L. PANGRAZZI,[a†‡] A. POLI,[a] P. SGADÒ,[a] N. BERARDI[b,c] AND Y. BOZZI[a,b*]

[a] *Laboratory of Molecular Neuropathology, Centre for Integrative Biology, University of Trento, Italy*

[b] *Institute of Neuroscience, CNR, Pisa, Italy*

[c] *NEUROFARBA Department, University of Florence, Italy*

Abstract—Mice lacking the homeodomain transcription factor Engrailed-2 (*En2*$^{-/-}$ mice) are a well-characterized model for autism spectrum disorders (ASD). *En2*$^{-/-}$ mice present molecular, neuropathological and behavioral deficits related to ASD, including down-regulation of ASD-associated genes, cerebellar hypoplasia, interneuron loss, enhanced seizure susceptibility, decreased sociability and impaired cognition. Specifically, impaired spatial learning in the Morris water maze (MWM) is associated with reduced expression of neurofibromin and increased phosphorylation of extracellular-regulated kinase (ERK) in the hippocampus of *En2*$^{-/-}$ adult mice. In the attempt to better understand the molecular cascades underlying neurofibromin-dependent cognitive deficits in *En2* mutant mice, we investigated the expression and phosphorylation of synapsin I (SynI; a major target of neurofibromin-dependent signaling) in the hippocampus of wild-type (WT) and *En2*$^{-/-}$ mice before and after MWM. Here we show that SynI mRNA and protein levels are down-regulated in the hippocampus of naïve and MWM-treated *En2*$^{-/-}$ mice, as compared to WT controls. This down-regulation is paralleled by reduced levels of SynI phosphorylation at Ser549 and Ser553 residues in the hilus of mutant mice, before and after MWM. These data indicate that in *En2*$^{-/-}$ hippocampus, neurofibromin-dependent pathways converging on SynI phosphorylation might underlie hippocampal-dependent learning deficits observed in *En2*$^{-/-}$ mice.

Key words: autism, mouse, ERK, learning, neurotransmission, synapse.

INTRODUCTION

The homeodomain transcription factor Engrailed-2 (*En2*) controls regionalization and patterning of the midbrain/hindbrain region (Joyner, 1996; Gherbassi and Simon, 2006). The human EN2 gene has been associated with autism spectrum disorders (ASD) (Gharani et al., 2004; Benayed et al., 2009), and abnormal expression of the EN2 gene has been reported in the cerebellum of ASD patients. Specifically, the EN2 intronic haplotype (rs1861972–rs1861973 A–C) associated with ASD has been shown to increase En2 protein expression in the cerebellum of ASD patients (Choi et al., 2012; James et al., 2013; Choi et al., 2014). In mice, a decreased En2 expression (that is, in opposite direction to the change observed in EN2 haplotype carriers) results in neuropathological and behavioral changes related to ASD. Mice lacking the *En2* homeodomain (*En2*$^{hd/hd}$; here referred to as *En2*$^{-/-}$) display cerebellar hypoplasia (Joyner et al., 1991; Kuemerle et al., 1997) and a reduced number of forebrain GABAergic interneurons (Tripathi et al., 2009; Sgadò et al., 2013a; Allegra et al., 2014) accompanied by ASD-like behaviors including enhanced seizure susceptibility (Tripathi et al., 2009), decreased sociability and impaired learning and memory (Cheh et al., 2006; Brielmaier et al., 2012; Provenzano et al., 2014).

Recent studies from our laboratory showed that *En2* is also widely expressed in postnatal forebrain, and indicate that it might control the structure and function of learning-related circuits (Tripathi et al., 2009; Sgadò et al., 2013a; Allegra et al., 2014; Provenzano et al., 2014). Indeed, spatial learning and memory deficits are very robust in *En2*$^{-/-}$ mice (Brielmaier et al., 2012; Provenzano et al., 2014) and might be relevant to cognitive impairment observed in ASD patients (Dawson et al., 2002). We recently showed that impaired spatial learning in the Morris water maze (MWM) is associated with reduced neurofibromin expression in the hippocampus of *En2*$^{-/-}$ adult mice (Provenzano et al., 2014). Neurofibromin is

*Correspondence to: Y. Bozzi, Centre for Integrative Biology (CIBIO), University of Trento, Via delle Regole 101, 38123 Mattarello, Trento, Italy. Tel: +39-0461-283651; fax: +39-0461-283937.
E-mail address: bozzi@science.unitn.it (Y. Bozzi).
† These authors equally contributed to this study.
‡ Present address: Research Institute for Biomedical Aging Research, University of Innsbruck, Austria.

Abbreviations: ASD, autism spectrum disorders; CA1/CA2/CA3, hippocampal pyramidal cell layers; Cdk5, cyclin-dependent kinase 5; *En2*, Engrailed-2; ERK, extracellular-regulated kinase; GABA, γ-aminobutyric acid; GCL, granule cell layer; mf, mossy fibers; MWM, Morris water maze; p-ERK, phosphorylated ERK; p-SynI, phosphorylated synapsin I; pyr, pyramidal cell layer; RT-qPCR, quantitative reverse-transcription polymerase chain reaction; slm, stratum lacunosum moleculare; s.r., stratum radiatum; SynI, synapsin I; SynII, synapsin II; WT, wild-type.

http://dx.doi.org/10.1016/j.neuroscience.2014.11.041
0306-4522/

coded by the NF1 gene, whose mutation is responsible of neurofibromatosis type 1, a complex genetic syndrome characterized by nervous system tumors and cognitive disabilities (Gutmann et al., 2012). Neurofibromin is a Ras-GTPase that negatively regulates extracellular-regulated kinase (ERK) phosphorylation (Fasano and Brambilla, 2011). Loss of neurofibromin function has been associated with learning deficits: mice with a *Nf1* heterozygous null mutation show enhanced ERK and synapsin I (SynI) phosphorylation resulting in increased GABA release in the hippocampus and impaired spatial learning (Cui et al., 2008).

Our recent studies suggest that neurofibromin-dependent pathways different from the canonical ERK–SynI cascade might underlie hippocampal-dependent learning deficits observed in $En2^{-/-}$ mice (Provenzano et al., 2014). In addition, SynI mRNA expression is down-regulated in $En2^{-/-}$ hippocampus (Sgadò et al., 2013b). Here, we further investigated SynI expression and phosphorylation in the hippocampus of wild-type (WT) and $En2^{-/-}$ mice following spatial learning test in the MWM, in the attempt to better understand the molecular cascades underlying neurofibromin-dependent cognitive deficits in *En2* mutant mice.

EXPERIMENTAL PROCEDURES

Animals

Experiments were conducted according to European Community Directive 2010/63/EU and approved by the Italian Ministry of Health. Animals were housed in a 12-h light/dark cycle with food and water available *ad libitum*. *En2* mutants, originally generated on a mixed 129 Sv × C57BL/6 genetic background (Joyner et al., 1991), were backcrossed at least five times on a C57BL/6 background (Sgadò et al., 2013a). WT and $En2^{-/-}$ mice were obtained through heterozygous ($En2^{+/-} \times En2^{+/-}$) mating. After weaning, animals were housed in groups, regardless of genotype (4–8 mice of the same sex per cage). Since learning behavior did not differ between genders in both WT and $En2^{-/-}$ mice (Brielmaier et al., 2012), male and female age-matched adult littermates (3–5 months old; weight = 25–35 g) were used. All animals used in this study came from the same MWM experiment described in Provenzano et al. (2014). Twenty-two mice (11 per genotype) were subjected to MWM and sacrificed at the end of the probe trial; for quantitative reverse-transcription polymerase chain reaction (RT-qPCR), four hippocampi per genotype were dissected and frozen in dry ice; for immunohistochemistry, four brains per genotype were fixed by 4% paraformaldehyde perfusion. Additional groups of age-matched, naïve mice (eight per genotype) were not subjected to MWM and used as controls. Their brains were dissected as above and used for RT-qPCR (four per genotype) and immunohistochemistry (four per genotype).

MWM

Experiments were performed as described in Provenzano et al. (2014). Briefly, mice were trained for nine days (two trials a day) to locate and escape onto a submerged platform in a circular tank (80 cm diameter) filled with opaque water (22 ± 1 °C). For each mouse, start position was pseudo-randomized across trials, and the hidden platform remained in the same quadrant for all trials across all training sessions. A spatial probe trial was performed 4 h after the last trial on day 9 of training; time spent, number of crossings and proximity to platform in all quadrants were scored. All animals were killed at the end of the spatial probe trial session and brains dissected. As compared to WT controls, $En2^{-/-}$ mice showed impaired learning during training sessions and lack of quadrant selectivity during probe trial (Provenzano et al., 2014).

Quantitative reverse transcription PCR

Hippocampal total RNAs were extracted and retrotranscribed as described (Provenzano et al., 2014). Quantitative reverse-transcription PCR (RT-qPCR) was performed in a real-time C1000 Thermal Cycler (BioRad Laboratories, Segrate, Italy) using the KAPA SYBR FAST Master Mix reagent (KAPA Biosystems, Wilmington, MA, USA). Primers were as follows: *SynI* forward 5′-ATGCAAACTCCACCCATCCTCAGA-3′, reverse 5′-AAGGAGGCCAAGTCAGTCACAGAT-3′ (NM_010897.2); mouse mitochondrial ribosomal protein *L41* (internal standard) forward 5′-GGTTCTCCCTTTCTCCCTTG-3′, reverse 5′-GCACCCCGACTCTTAGTGAA-3′ (NM_001031808.2). Ratios of comparative concentrations of *Syn I* mRNA with respect to *L41* mRNA were then calculated and plotted as the average of three independent reactions with technical replicates obtained from each RNA pool. Expression analyses were performed using the CFX3 Manager software (BioRad Laboratories, Segrate, Italy).

Immunohistochemistry, densitometry and cell counts

All animals from the four experimental groups were sacrificed on the same day, at the end of MWM session (Provenzano et al., 2014). All brains were fixed by transcardial perfusion with the same batch of 4% paraformaldehyde followed by 1-h post-fixation. Vibratome-cut (40-μm thick) serial coronal sections taken at the level of dorsal hippocampus were incubated the following primary antibodies: goat polyclonal anti-SynIa/b (*N*−19) (Santa-Cruz Biotechnology, Heidelberg, Germany sc-7379; 1:200 dilution), rabbit polyclonal anti-phosphorylated ERK1/2 (Cell Signaling Technologies, Leiden, The Netherlands 4370, 1:500 dilution), rabbit polyclonal anti-neurofibromin (SantaCruz Biotechnology, Heidelberg, Germany sc-67, 1:100 dilution), rabbit polyclonal anti-phosphorylated SynI (anti-p-SynI) (Ser549) (Novus Biologicals, Littleton, CO, USA NB300-744; 1:300 dilution), goat polyclonal anti-p-SynI a/b (Ser553) (SantaCruz Biotechnology, Heidelberg, Germany sc-12913; 1:200 dilution). Following incubation with primary antibodies, appropriate biotin-conjugated secondary antibodies were incubated with streptavidin-conjugated fluorophores (AlexaFluor 488/594, Life Technologies Italia, Monza, Italy) for immunofluorescence or avidin–biotin-peroxidase complex (ABC kit, Vector Laboratories, USA) for diaminobenzidine (DAB) staining. Tissues representing all four experimental

groups were processed for immunocytochemistry at the same time with the same batches of reagents.

Quantification of immunohistochemistry experiments was performed as described (Sgadò et al., 2013a; Provenzano et al., 2014). For densitometric analysis of SynI staining, acquired black and white images were inverted. Two separate contours were drawn for each digital image: positive staining was calculated in the entire mossy fiber pathway (from the hilus to the CA3 region), whereas background was calculated over the corpus callosum. Mean optical density values (normalized to contour area) were calculated by subtracting the non-specific background to SynI-specific signal in mossy fibers (mf). To count p-SynI-positive cells, three sections at the level of dorsal hippocampus were analyzed per animal. Multiple bright-field images from each section were acquired at 20× magnification using a Zeiss AxioImager M2 microscope, and then assembled using Adobe Photoshop. Light intensity and microscope settings were optimized initially and then kept constant to maintain the same exposure for collecting images representing all four experimental groups. Cell counts were then performed on tiff-converted mosaic images using ImageJ (http://rsb.info.nih.gov/ij/). Stained cells were counted in the different hippocampal subfields over a minimum of three counting boxes of 100 × 100 μm each. Cell densities were expressed as the number of labeled cells per counting window (100 × 100 μm). All counts and measurements were performed by an experimenter blind of genotypes.

Statistical analysis

Statistical analyses were performed by GraphPad software. Two-way ANOVA followed by appropriate multiple comparisons post hoc tests were used, with statistical significance level set at $p < 0.05$. Values are reported as mean ± s.e.m.

RESULTS

We recently reported that in *En2*$^{-/-}$ mice spatial learning deficits in MWM are accompanied by neurofibromin signaling deficits (Provenzano et al., 2014). Specifically, our study suggests that neurofibromin-dependent pathways different from the canonical ERK–SynI cascade might underlie hippocampal-dependent learning deficits observed in *En2*$^{-/-}$ mice. Here we used brain samples from the same animals used in our previous study (Provenzano et al., 2014) to further investigate SynI phosphorylation in the hippocampus of WT and *En2*$^{-/-}$ mice before and after MWM. *En2*$^{-/-}$ mice showed impaired learning in MWM compared to WT controls (Provenzano et al., 2014).

SynI mRNA expression is down-regulated in the *En2*$^{-/-}$ hippocampus

We first investigated *SynI* mRNA expression in WT and *En2*$^{-/-}$ mice before and after the MWM test. To this purpose, we first performed RT-qPCR experiments using the mitochondrial ribosomal L41 protein mRNA as a standard for quantification. As expected, L41

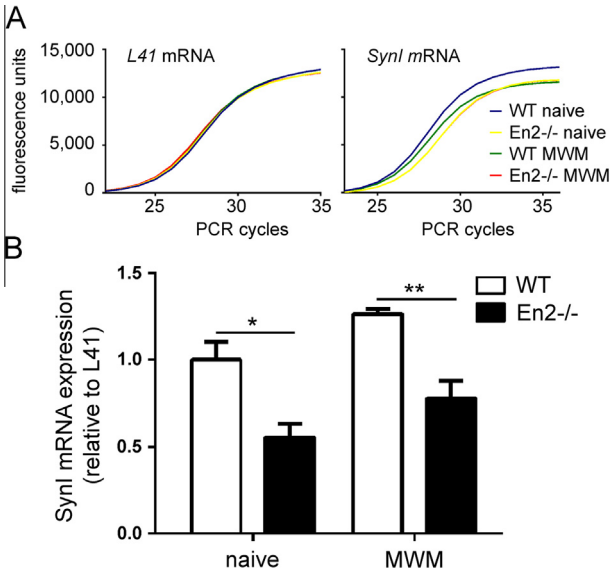

Fig. 1. *SynI* mRNA levels in the hippocampus of WT and *En2*$^{-/-}$ before and after MWM training. (A) Real-time RT-PCR amplification profiles of mitochondrial ribosomal protein *L41* (housekeeping gene) and *SynI* mRNAs from WT and *En2*$^{-/-}$ hippocampi, before and after MWM (as indicated). The graphs report the appearance of fluorescence (arbitrary units) in PCR amplicons as a function of the number of PCR cycles. The scale of y axis is the same in both graphs. No difference in *L41* mRNA expression was detected across the four experimental groups. (B) Quantification of *SynI* mRNA expression in the hippocampus of WT and En2$^{-/-}$ mice, before (naïve) and after MWM. *SynI* mRNA levels are normalized to *L41* mRNA $^{*}p < 0.05$, $^{**}p < 0.001$ (two-way ANOVA followed by Tukey's post hoc test; $n = 4$ per genotype per treatment group).

amplification gave comparable amplification curves in all analyzed samples, independent of genotype and treatment (Fig. 1A). In keeping with our previous findings (Sgadò et al., 2013b), RT-qPCR experiments revealed a significant difference in *SynI* mRNA levels between genotypes but not training groups [two-way ANOVA, main effect of genotype, $F_{(1,15)} = 32.41$, $p = 0.0002$; main effect of training, $F_{(1,15)} = 9.013$, $p = 0.01$]. Lower levels of SynI mRNA were detected in the hippocampus of *En2*$^{-/-}$ naïve mice compared to WT (Tukey's post hoc test, $p < 0.05$; $n = 4$ per genotype; Fig. 1). SynI mRNA levels remained lower in *En2*$^{-/-}$ mice after MWM (Tukey's post hoc test, $p < 0.01$; $n = 4$ per genotype; Fig. 1B, C).

SynI protein levels are reduced in the *En2*$^{-/-}$ hippocampus

SynI expression in WT and *En2*$^{-/-}$ hippocampus was then investigated at the protein level. Immunohistochemistry experiments were performed using an antibody raised against the N-terminal of SynI, recognizing both the non-phosphorylated and phosphorylated forms of the protein (see Experimental Procedures). In agreement with mRNA data, immunohistochemistry experiments revealed a lower SynI staining throughout the whole dorsal hippocampus of *En2*$^{-/-}$ naïve mice, as compared to WT (Fig. 2A). In both genotypes, SynI immunostaining was localized in fiber compartments (e.g., stratum radiatum (s.r.), mf), whereas CA1/CA3 pyramidal cell layers and granule cell layer (GCL) did not show any

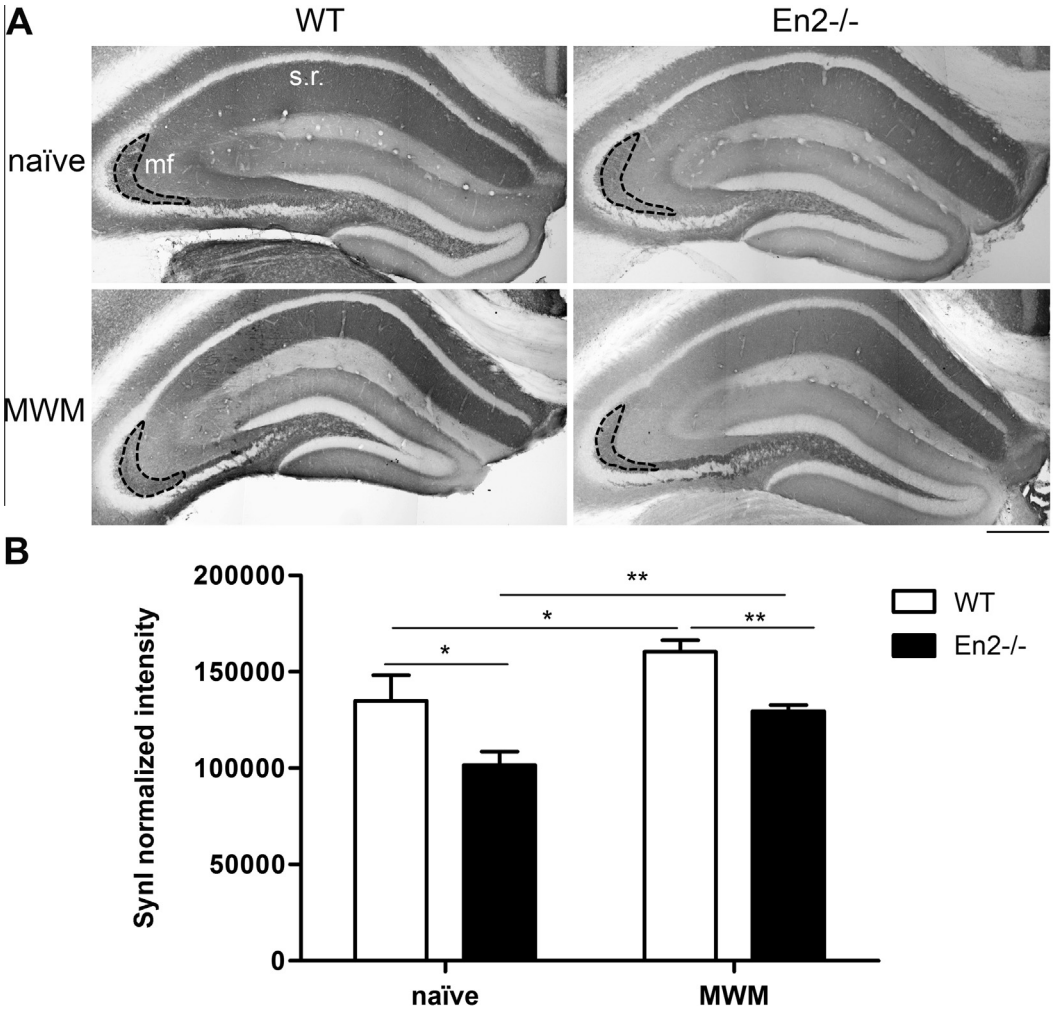

Fig. 2. SynI protein levels in the hippocampus of WT and *En2*$^{-/-}$ before and after MWM training. (A) Representative SynI immunostainings on the whole dorsal hippocampus of WT and *En2*$^{-/-}$ mice, before (naïve) and after MWM. Dashed lines outline the areas used for mossy fiber staining quantification. Scale bar = 400 μm. *Abbreviations:* mf, mossy fibers; s.r., stratum radiatum. (B) Densitometric analysis of SynI immunostaining in the mossy fiber pathway from the four experimental groups. Densitometry was performed on the areas outlined in A), where signals were linear and not saturated. $^{*}p < 0.05$, $^{**}p < 0.01$ (two-way ANOVA followed by Tukey's post hoc test; $n = 4$ per genotype and treatment group). Genotypes and treatments are as indicated.

labeling (Fig. 2A). SynI immunostaining in fiber compartments increased after MWM in both genotypes, but remained lower in *En2*$^{-/-}$ mice, as compared to WT (Fig. 2A). Densitometric analysis in mf confirmed a significant effect of both genotype and training [two-way ANOVA, main effect of training, $F_{(1,47)} = 11,47$, $p = 0.0018$; main effect of genotype, $F_{(1,45)} = 16.61$, $p = 0.0003$; Tukey's post hoc test, $p < 0.05$ for WT naïve vs *En2*$^{-/-}$ naïve and WT naïve vs WT MWM; $p < 0.01$ for *En2*$^{-/-}$ naïve vs *En2*$^{-/-}$ MWM and WT MWM vs *En2*$^{-/-}$ MWM; $n = 4$ per genotype and treatment group] (Fig. 2B).

Down-regulation of *SynI* phosphorylation (Ser549) in the hilus of *En2*$^{-/-}$ mice

Our recent study (Provenzano et al., 2014) suggests that neurofibromin-dependent pathways different from the canonical ERK–SynI cascade are implicated in hippocampal-dependent learning deficits observed in *En2*$^{-/-}$ mice. Indeed, phospho-ERK (p-ERK) staining in naïve WT mice was mainly restricted to mf, where it co-localized with SynI staining (Fig. 3A, B). CA1/CA3 pyramidal cell layers and GCL), which did not show SynI labeling (Figs. 2A and 3A, B), were also devoid of p-ERK staining (Fig. 3A, B).

We then investigated the profile of SynI phosphorylation in the hippocampus of WT and *En2*$^{-/-}$ mice before and after MWM, using specific antibodies that recognize ERK-dependent (Ser549; Jovanovic et al., 1996) and ERK-independent (Ser553; Matsubara et al., 1996) phosphorylation sites on SynI.

Immunohistochemistry for p-SynI (Ser549 residue) revealed a widespread staining throughout the whole dorsal hippocampus of WT and *En2*$^{-/-}$ mice before and after MWM (Fig. 4A). In both genotypes and experimental conditions, staining was mainly localized to cell bodies. p-SynI (Ser549)-positive fibers in mf and CA1 s.r. were clearly visible in WT naïve animals,

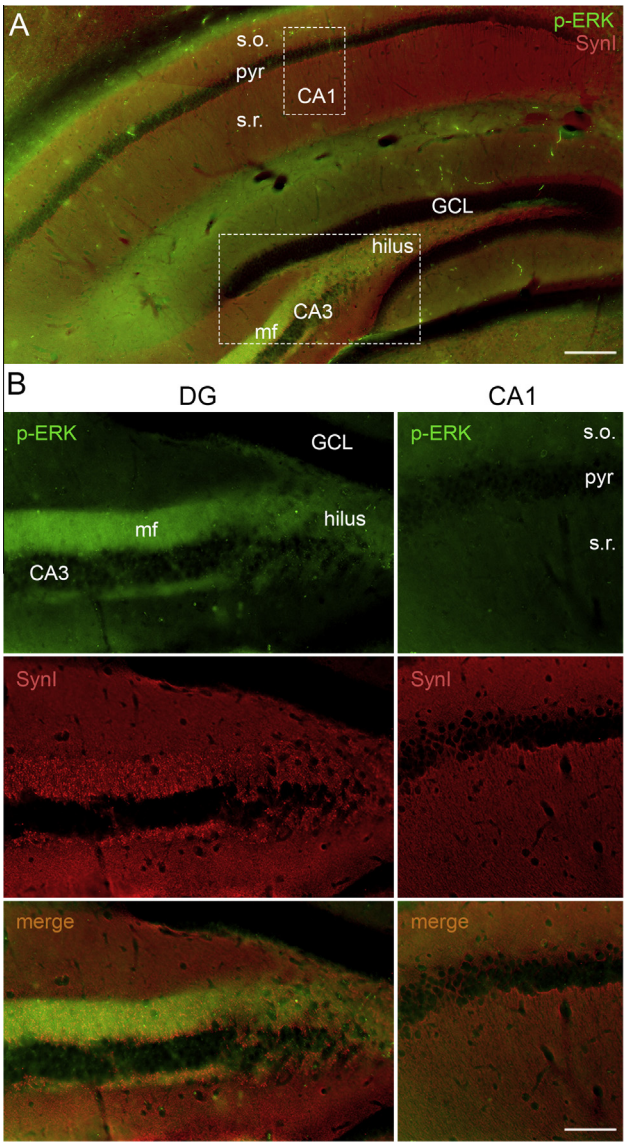

Fig. 3. SynI and p-ERK expression in the WT hippocampus. (A) Representative double immunostaining of p-ERK (green) and SynI (red). Picture shows a low magnification of dentate gyrus and mossy fibers from a WT mouse. Dashed lines indicates the dentate gyrus (DG) and CA1 areas shown in B. (B) Details of p-ERK (green), SynI (red) and merged (orange) immunostainings from DG and CA1 subfields. *Abbreviations:* CA1/CA3, pyramidal layers; DG, dentate gyrus; GCL, granule cell layer; mf, mossy fibers; pyr, stratum pyramidale; s.o., stratum oriens; s.r., stratum radiatum. Scale bars = 150 μm (A), 80 μm for DG in (B) and 100 μm for CA1 in (B). (For interpretation of the references to color in this figure legend, the reader is referred to the web version of this article.)

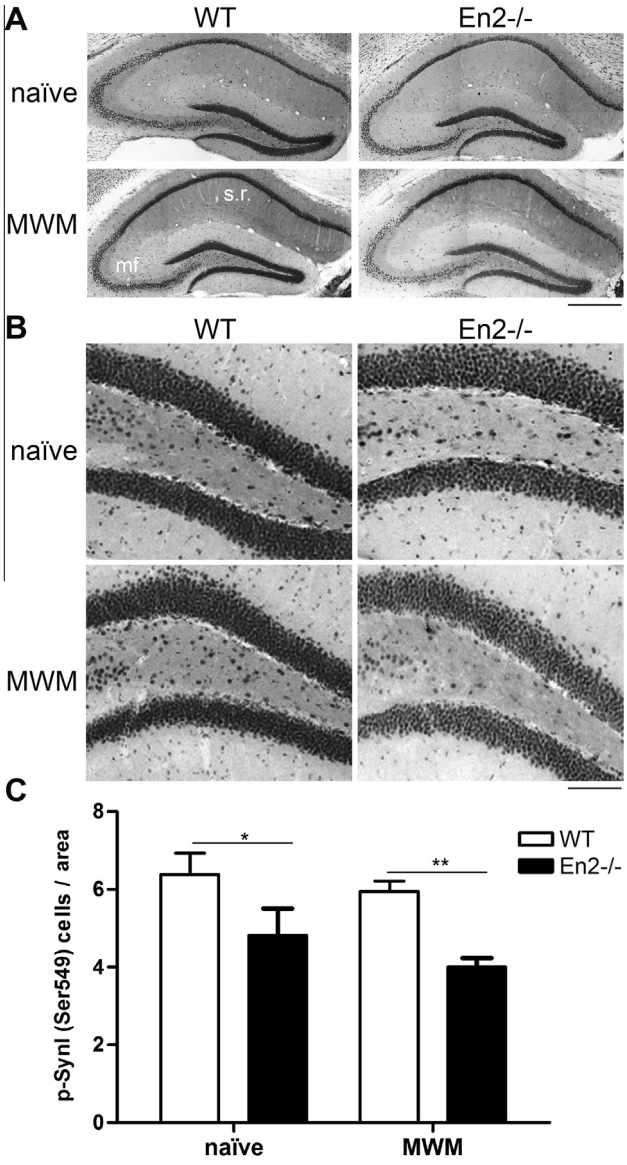

Fig. 4. Levels of p-SynI (Ser549) in the hippocampus of WT and *En2*$^{-/-}$ before and after MWM training. (A, B) Representative p-SynI (Ser549) immunostainings on the whole dorsal hippocampus (A) and hilus (B) of WT and *En2*$^{-/-}$ mice, before (naïve) and after MWM. Scale bars = 100 μm (A), 400 μm (B). *Abbreviations:* mf, mossy fibers; s.r., stratum radiatum. (C) Counts of p-SynI (Ser549)-positive cells in the hilus from the four experimental groups. $^{*}p < 0.05$, $^{**}p < 0.01$ (two-way ANOVA followed by Tukey's post hoc test; $n = 4$ per genotype and treatment group). Genotypes and treatments are as indicated.

whereas naïve *En2*$^{-/-}$ mice showed a very faint fiber staining (Fig. 4A). Interestingly, a lower number of p-SynI (Ser549)-positive cells was detected in the hilus of *En2*$^{-/-}$ naïve mice compared to WT controls [two-way ANOVA, main effect of genotype $F_{(1,45)} = 13.42$, $p = 0.0008$; Tukey's post hoc test, $p < 0.05$ for WT naïve vs *En2*$^{-/-}$ naïve, $p < 0.01$ for WT MWM vs *En2*$^{-/-}$ MWM; $n = 4$ per genotype and treatment group; Fig. 4B, C]. Similarly, a lower number of p-SynI (Ser549)-positive cells was also detected in the stratum lacunosum moleculare (slm) of *En2*$^{-/-}$ mice as compared to WT [two-way ANOVA, main effect of genotype $F_{(1,45)} = 9.609$, $p = 0.0037$; Tukey's post hoc test, $p < 0.01$ for WT naïve vs *En2*$^{-/-}$ naïve, $p < 0.05$ for WT MWM vs *En2*$^{-/-}$ MWM; $n = 4$ per genotype and treatment group; data not shown].

Down-regulation of *SynI* phosphorylation (Ser553) in the hilus of *En2*$^{-/-}$ mice

We next investigated the profile of SynI phosphorylation on Ser553 residue, which is known to be dependent on cyclin-dependent kinase 5 (Cdk5) (Matsubara et al.,

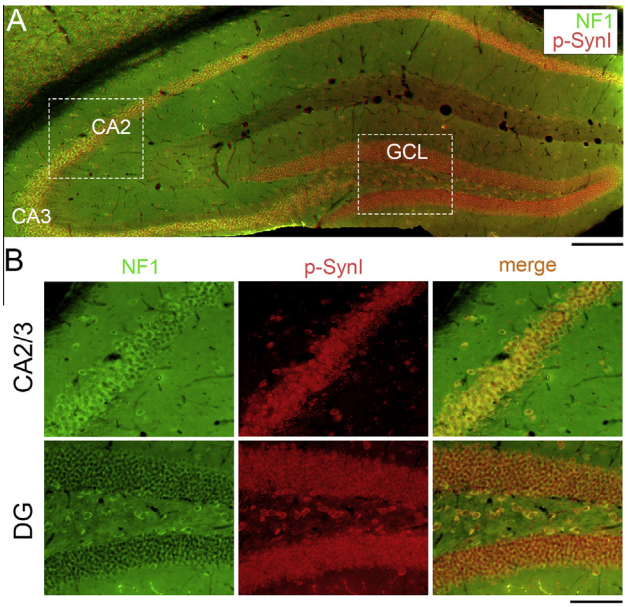

Fig. 5. p-SynI (Ser553) and neurofibromin expression in the WT hippocampus. (A) Low magnification of the dorsal hippocampus from a WT mouse, stained for NF1 (green) and p-SynI (Ser553) (red). Dashed lines indicate the areas shown in B. (B) High magnification of the CA2/3 and DG subfields, showing NF1 (green), p-SynI (red) and double (merged) immunostainings. *Abbreviations:* CA3, pyramidal layer; GCL, granule cell layer; mf, mossy fibers. Scale bars = 200 μm (A), 80 μm (B). (For interpretation of the references to color in this figure legend, the reader is referred to the web version of this article.)

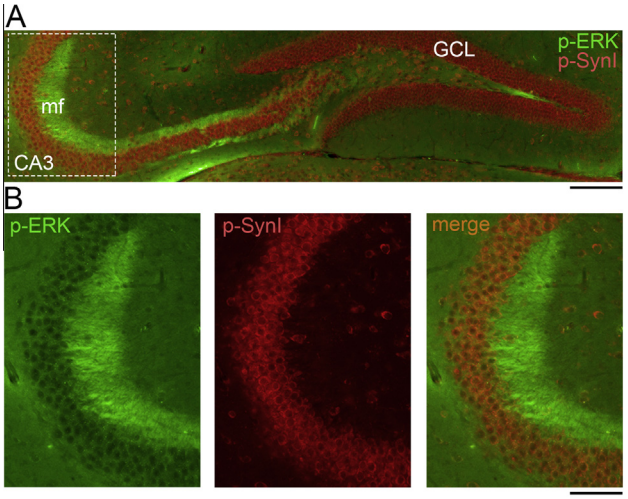

Fig. 6. p-SynI (Ser553) and p-ERK expression in the WT hippocampus. (A) Picture shows a low magnification of the dorsal hippocampus from a WT mouse, stained for p-ERK (green) and p-SynI (Ser553) (red). The dashed line indicates the area shown in B. (B) High magnification of the CA3 subfield, showing p-ERK (green), p-SynI (red) and double (merged) immunostainings. *Abbreviations:* CA3, pyramidal layer; GCL, granule cell layer; mf, mossy fibers. Scale bars = 150 μm (A), 80 μm (B). (For interpretation of the references to color in this figure legend, the reader is referred to the web version of this article.)

1996). Indeed, p-SynI (Ser553) staining co-localized with neurofibromin (Fig. 5) but not p-ERK (Fig. 6) in the hippocampus of naïve WT mice.

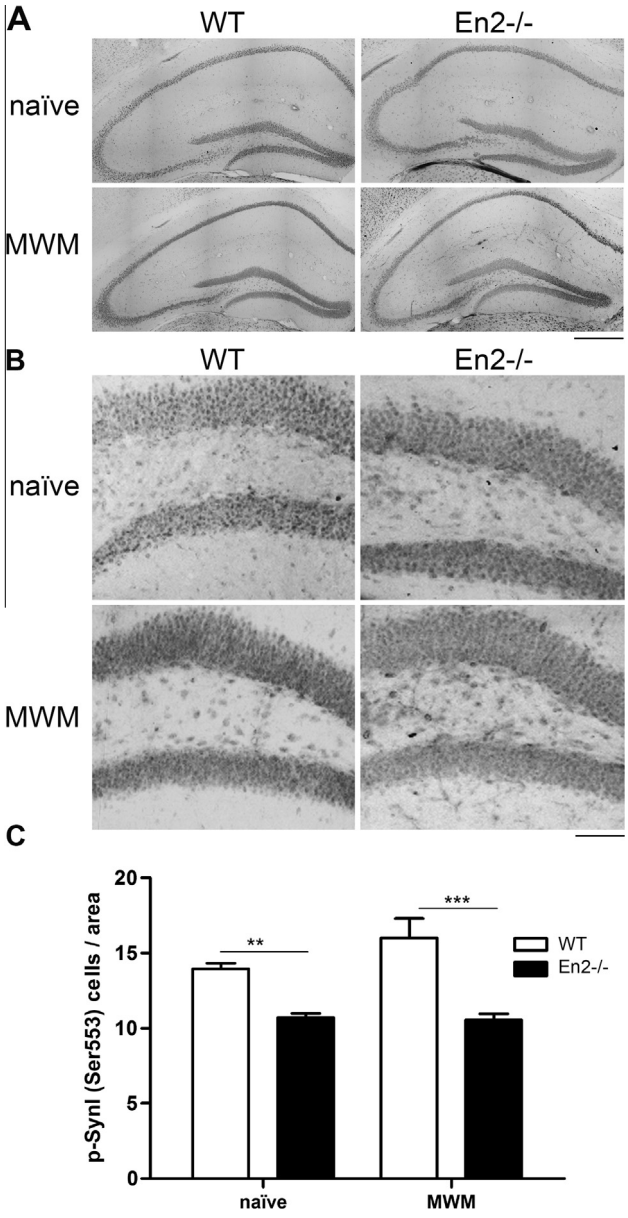

Fig. 7. Levels of p-SynI (Ser553) in the hippocampus of WT and *En2*$^{-/-}$ before and after MWM training. (A, B) Representative p-SynI (Ser553) immunostainings on the whole dorsal hippocampus (A) and hilus (B) of WT and *En2*$^{-/-}$ mice, before (naïve) and after MWM. Scale bar = 100 μm (A), scale bar = 400 μm (B). C) Counts of p-SynI (Ser553)-positive cells in the hilus from the four experimental groups. $^{**}p < 0.01$, $^{***}p < 0.001$ (two-way ANOVA followed by Tukey's post hoc test; $n = 4$ per genotype and treatment group). Genotypes and treatments are as indicated.

Immunohistochemistry for p-SynI (Ser553) showed a widespread staining throughout the whole dorsal hippocampus of WT and *En2*$^{-/-}$ mice before and after MWM, with a staining localized to cell bodies (Fig. 7A). Quantification of p-SynI (Ser553)-positive cells in GCL revealed no differences across genotypes in both naïve and MWM-trained groups [GCL: two-way ANOVA, main effect of genotype $F_{(1,45)} = 0.543$, $p = 0.46$; $n = 4$ per genotype and treatment group; data not shown]. A significantly lower number of p-SynI (Ser553)-positive

cells was detected in the hilus of *En2*$^{-/-}$ mice compared to WT controls, in both naïve and MWM conditions [two-way ANOVA, main effect of genotype $F_{(1,45)} = 39.26$, $p < 0.0001$; Tukey's post hoc test, $p < 0.01$ for WT naïve vs *En2*$^{-/-}$ naïve, $p < 0.001$ for WT MWM vs *En2*$^{-/-}$ MWM; $n = 4$ per genotype and treatment group] (Fig. 7B, C). A lower number of p-SynI (Ser553)-positive cells was also detected in slm of *En2*$^{-/-}$ mice as compared to WT, in both naïve and MWM animals [two-way ANOVA, main effect of genotype $F_{(1,45)} = 25.91$, $p = 0.0001$; main effect of training $F_{(1,45)} = 174.9$, $p = 0.0001$; Tukey's post hoc test, $p < 0.01$ for WT naïve vs *En2*$^{-/-}$ naïve; $p = 0.002$ for WT MWM vs *En2*$^{-/-}$ MWM; $n = 4$ per genotype and treatment group; data not shown].

DISCUSSION

In this study, we showed that *SynI* mRNA and protein levels are down-regulated in the hippocampus of *En2*$^{-/-}$ adult mice. This down-regulation was accompanied by reduced levels of SynI phosphorylation (Ser549/553) in the hilus of both naïve and MWM-treated mutant mice, indicating that multiple pathways converging on SynI phosphorylation might underlie learning deficits in *En2*$^{-/-}$ mice.

Synapsins are a family of neuronal phosphoproteins involved in neural development, synaptic transmission and plasticity. Their best-characterized function is to control synaptic vesicle trafficking and modulate neurotransmitter release at the pre-synaptic terminal (Cesca et al., 2010). Mutations in Syn genes have been associated with ASD (Fassio et al., 2011; Corradi et al., 2014); accordingly, Syn knockout mice display ASD-like features, including reduced social interactions and repetitive behaviors (Greco et al. 2013). In addition, both *SynI*$^{-/-}$ and *SynII*$^{-/-}$ mice display spatial and emotional memory deficits, as evaluated by object recognition and fear-conditioning tests, respectively (Corradi et al., 2008). These deficits are accompanied by neuronal loss and gliosis in the cerebral cortex and hippocampus (Corradi et al., 2008).

We recently showed by microarray and RT-qPCR analyses that SynI mRNA levels are down-regulated in the hippocampus of *En2*$^{-/-}$ adult mice (Sgadò et al., 2013b). SynI is one of the several ASD-related genes whose expression is down-regulated in *En2*$^{-/-}$ mice, indicating that the molecular signature of the *En2*$^{-/-}$ brain shares convergent pathological pathways with ASD (Sgadò et al., 2013b). Here we confirmed and extended these data, showing a 40% and 30% reduction of *SynI* mRNA and protein levels, respectively, in the *En2*$^{-/-}$ hippocampus (Figs. 1 and 2). It is interesting to point out that *En2*$^{-/-}$ mice, which present lower levels of hippocampal SynI, display spatial memory (object recognition) deficits (Brielmaier et al., 2012), as observed in *SynI* knockout mice (Corradi et al., 2008).

In a recent study, we showed that impaired spatial learning performance in the MWM is associated with a 50% reduction of neurofibromin protein in the hippocampus of *En2*$^{-/-}$ adult mice (Provenzano et al., 2014). In mice, loss of neurofibromin (a negative regulator of ERK function) results in increased ERK/SynI phosphorylation, enhanced GABA transmission in the hippocampus and impaired spatial learning (Cui et al., 2008). Our recent and present studies suggest that neurofibromin-dependent pathways different from the canonical ERK–SynI cascade might be involved hippocampal-dependent learning deficits detected in *En2*$^{-/-}$ mice: the number of hippocampal neurons co-expressing neurofibromin and p-ERK is very low in *En2*$^{-/-}$ mice, and an increased number of p-ERK-positive neurons was also detected in subfields of the *En2*$^{-/-}$ hippocampus where neurofibromin down-regulation was not detected (Provenzano et al., 2014). In addition, SynI levels are down-regulated (Sgadò et al., 2013b; this study, Fig. 1). Data present in the literature suggest that neurofibromin might also regulate SynI phosphorylation independently of ERK. One kinase possibly involved in this regulation is the cdk5. Cdk5 is known to phosphorylate SynI (see below; Giovedí et al., 2014), and neurofibromin has been shown to interact with cdk5 to regulate the phosphorylation of cellular substrates (such as the collapsin response mediator protein-2, CRMP-2; Lin and Hsueh, 2008; Patrakitkomjorn et al., 2008).

All Syn isoforms share a conserved structure, subdivided in different functional domains (named A–E, from the NH_2 to the COOH terminus). Most of these domains contain consensus sequences for protein kinase-dependent phosphorylation, which constitute the regulatory sites of Syn function (Cesca et al., 2010; Giovedí et al., 2014). Domain A contains phosphorylation sites for protein kinase A, PKA and Ca^{2+}/calmodulin-dependent kinases (CaMK), whereas ERK-dependent sites are located in the B domain; phosphorylation at these sites modulates the reversible association of Syn with synaptic vesicles. The C domain is responsible for Syn interaction with actin filaments and synaptic vesicles, and is phosphorylated by the tyrosine kinase Src. Finally, the D domain (which is specific for SynIa/b isoforms) contains cdk1/5-dependent phosphorylation sites, as well as additional phosphorylation sites for CaMKII and ERK, and regulates SynI binding to actin and synaptic vesicles (Giovedí et al., 2014).

In this study, we used p-SynI-specific antibodies that recognize ERK dependent (Ser549; Jovanovic et al. 1996) and cdk5-dependent (Ser553; Matsubara et al., 1996) phosphorylation sites in the D domain. In *En2*$^{-/-}$ mice, we found a lower number of p-SynI (Ser 549)-positive cells in the hilus and slm, and fewer p-SynI (Ser553)-positive cells in the hilus. Reduced levels of SynI expression and phosphorylation lead to cognitive deficits; SynI mutant mice display impaired hippocampal-dependent learning (Corradi et al., 2008). In addition, lower SynI/p-SynI levels are present in the hippocampus of animals with poor cognitive performance, indicating a positive correlation between hippocampal SynI/p-SynI levels and hippocampal-dependent behaviors (Resende et al., 2012). Conversely, SynI phosphorylation is increased by long-term potentiation (Nayak et al., 1996), and exercise-induced improvement of cognitive performance in MWM

is paralleled by increased hippocampal p-Syn (Molteni et al., 2004; Griesbach et al., 2009). In accordance with these findings, we showed a lower number of SynI- and p-SynI-positive cells in the hippocampus of *En2*$^{-/-}$ mice, which display robust spatial learning deficits (Brielmaier et al., 2012; Provenzano et al., 2014). We also showed that SynI immunostaining in both WT and *En2*$^{-/-}$ hippocampus is restricted to fiber compartments (as previously observed by other authors using the same SynI antibody; Nowicka et al., 2003), and this staining is reduced in mf (Fig. 2). p-SynI staining was instead well detectable in pyramidal and granule cell bodies in both genotypes (Figs. 4–7). Upon phosphorylation, SynI has generally been shown to translocate from nerve terminal to the cytosol (Sihra et al., 1989; Chi et al., 2001). However, other authors (using the same p-SynI Ser553 antibody reported in this study) could detect p-SynI staining in the cell bodies of hippocampal pyramidal neurons (Meng et al., 2006). It remains to be explained why intense p-SynI staining was detected in pyramidal cell bodies, where we could not detect any total protein (Fig. 2). A possible explanation is that p-SynI has a conformation that does not allow it to be recognized by the SynI antibody. In addition, we cannot exclude the possibility that the p-SynI antibody recognizes other phosphorylated proteins such as other members of the synapsin family. Phosphorylation at Ser553 residue is known to reduce SynI ability to interact with actin, while leaving its interaction with microtubules unaffected (Matsubara et al., 1996). As proposed by other authors (Meng et al., 2006), p-SynI might then be free to leave the synaptic terminal, translocating to the cell soma. It interesting to note that somatic localization of SynI has been detected in retinal ganglion cells at early postnatal stages, before complete maturation of retinal circuits (Haas et al., 1990). This suggests that somatic localization of SynI might relate to an immature state of neuronal function. However, the role of p-SynI in the soma of hippocampal neurons remains to be elucidated.

Finally, training in the MWM induced a detectable increase of SynI and p-SynI immunoreactivity in the same areas in WT but not *En2*$^{-/-}$ mice (Figs. 2 and 4), confirming that hippocampal activity during learning results in widespread induction of SynI expression and phosphorylation in hippocampal fiber layers. Increased SynI phosphorylation associated with enhanced cognitive performance has been generally ascribed to activation of ERK signaling. Indeed, increased ERK-dependent phosphorylation of SynI in transgenic mice overexpressing a constitutively active form of H-ras resulted in enhanced cognitive performance, which is blocked by deletion of *SynI* (Kushner et al., 2005). Our results, showing reduced levels of both ERK-dependent and ERK-independent SynI phosphorylation in the *En2*$^{-/-}$ hippocampus, suggest that multiple signaling pathways converge onto SynI to impair hippocampal-dependent learning; in addition, the co-localization of p-SynI (Ser553) staining with neurofibromin but not p-ERK in pyramidal and granule cell layers (Figs. 5 and 6), suggests that neurofibromin-dependent pathways might lead to SynI phosphorylation independently of ERK activation.

CONCLUSIONS

In this study, we showed that *SynI* mRNA and protein levels are down-regulated in the hippocampus of *En2*$^{-/-}$ mice, both before and after a spatial learning test. This down-regulation is paralleled by reduced SynI phosphorylation at Ser549/553 residues in the hilus of mutant mice, indicating that in the *En2*$^{-/-}$ hippocampus different signaling pathways converge onto SynI to impair hippocampal-dependent learning.

Acknowledgments—We are grateful to the technical/administrative staff of the CIBIO and CNR Neuroscience Institute assistance. This work was funded by the Italian Ministry of University and Research (PRIN 2008 grant # 200894SYW2_002 and PRIN 2010–2011 grant # 2010N8PBAA_002 to Y.B.) and University of Trento (CIBIO start-up grant to Y.B.). P.S. is supported by Provincia Autonoma di Trento (Italy) under the Marie Curie-People cofunding action of the European Community. The authors declare no competing financial interests.

REFERENCES

Allegra M, Genovesi S, Maggia M, Cenni MC, Zunino G, Sgadò P, Caleo M, Bozzi Y (2014) Altered GABAergic markers, increased binocularity and reduced plasticity in the visual cortex of Engrailed-2 knockout mice. Front Cell Neurosci 8:163. http://dx.doi.org/10.3389/fncel.2014.00163.

Benayed R, Choi J, Matteson PG, Gharani N, Kamdar S, Brzustowicz LM, Millonig JH (2009) Autism-associated haplotype affects the regulation of the homeobox gene, ENGRAILED 2. Biol Psychiatry 66:911–917.

Brielmaier J, Matteson PG, Silverman JL, Senerth JM, Kelly S, Genestine M, Millonig JH, Dicicco-Bloom E, Crawley JN (2012) Autism-relevant social abnormalities and cognitive deficits in Engrailed-2 knockout mice. PLoS One 7:e40914. http://dx.doi.org/10.1371/journal.pone.0040914.

Cesca F, Baldelli P, Valtorta F, Benfenati F (2010) The synapsins: key actors of synapse function and plasticity. Prog Neurobiol 91:313–348.

Cheh MA, Millonig JH, Roselli LM, Ming X, Jacobsen E, Kamdar S, Wagner GC (2006) En2 knockout mice display neurobehavioral and neurochemical alterations relevant to autism spectrum disorder. Brain Res 1116:166–176.

Chi P, Greengard P, Ryan TA (2001) Synapsin dispersion and reclustering during synaptic activity. Nat Neurosci 4:1187–1193.

Choi J, Ababon MR, Matteson PG, Millonig JH (2012) Cut-like homeobox 1 and nuclear factor I/B mediate ENGRAILED2 autism spectrum disorder-associated haplotype function. Hum Mol Genet 21:1566–1580.

Choi J, Ababon MR, Soliman M, Lin Y, Brzustowicz LM, Matteson PG, Millonig JH (2014) Autism associated gene, engrailed2, and flanking gene levels are altered in post-mortem cerebellum. PLoS One 9(2):e87208. http://dx.doi.org/10.1371/journal.pone.0087208.

Corradi A, Zanardi A, Giacomini C, Onofri F, Valtorta F, Zoli M, Benfenati F (2008) Synapsin-I- and synapsin-II-null mice display an increased age-dependent cognitive impairment. J Cell Sci 121:3042–3051.

Corradi A, Fadda M, Piton A, Patry L, Marte A, Rossi P, Cadieux-Dion M, Gauthier J, Lapointe L, Mottron L, Valtorta F, Rouleau GA, Fassio A, Benfenati F, Cossette P (2014) SYN2 is an autism predisposing gene: loss-of-function mutations alter synaptic vesicle cycling and axon outgrowth. Hum Mol Genet 23:90–103.

Cui Y, Costa RM, Murphy GG, Elgersma Y, Zhu Y, Gutmann DH, Parada LF, Mody I, Silva AJ (2008) Neurofibromin regulation of ERK signaling modulates GABA release and learning. Cell 135:549–560.

Dawson G, Webb S, Schellenberg GD, Dager S, Friedman S, Aylward E, Richards T (2002) Defining the broader phenotype of autism: genetic, brain, and behavioral perspectives. Dev Psychopathol 14:581–611.

Fasano S, Brambilla R (2011) Ras-ERK signaling in behavior: old questions and new perspectives. Front Behav Neurosci 5:79. http://dx.doi.org/10.3389/fnbeh.2011.00079.

Fassio A, Patry L, Congia S, Onofri F, Piton A, Gauthier J, Pozzi D, Messa M, Defranchi E, Fadda M, Corradi A, Baldelli P, Lapointe L, St-Onge J, Meloche C, Mottron L, Valtorta F, Khoa Nguyen D, Rouleau GA, Benfenati F, Cossette P (2011) SYN1 loss-of-function mutations in autism and partial epilepsy cause impaired synaptic function. Hum Mol Genet 20:2297–2307.

Gharani N, Benayed R, Mancuso V, Brzustowicz LM, Millonig JH (2004) Association of the homeobox transcription factor, ENGRAILED 2, with autism spectrum disorder. Mol Psychiatry 9:474–484.

Gherbassi D, Simon HH (2006) The engrailed transcription factors and the mesencephalic dopaminergic neurons. J Neural Transm Suppl 70:47–55.

Giovedí S, Corradi A, Fassio A, Benfenati F (2014) Involvement of synaptic genes in the pathogenesis of autism spectrum disorders: the case of synapsins. Front Pediatr 2:94. http://dx.doi.org/10.3389/fped.2014.00094.

Greco B, Managò F, Tucci V, Kao H-T, Valtorta F, Benfenati F (2013) Autism-related behavioral abnormalities in synapsin knockout mice. Behav Brain Res 251:65–74.

Griesbach GS, Hovda DA, Gomez-Pinilla F (2009) Exercise-induced improvement in cognitive performance after traumatic brain injury in rats is dependent on BDNF activation. Brain Res 1288:105–115.

Gutmann DH, Parada LF, Silva AJ, Ratner N (2012) Neurofibromatosis type 1: modeling CNS dysfunction. J Neurosci 32:14087–14093.

Haas CA, DeGennaro LJ, Müller M, Holländer H (1990) Synapsin I expression in the rat retina during postnatal development. Exp Brain Res 82:25–32.

James SJ, Shpyleva S, Melnyk S, Pavliv O, Pogribny IP (2013) Complex epigenetic regulation of Engrailed-2 (EN-2) homeobox gene in the autism cerebellum. Transl Psychiatry 3:e232. http://dx.doi.org/10.1038/tp.2013.8.

Joyner AL (1996) Engrailed, Wnt and Pax genes regulate midbrain–hindbrain development. Trends Genet 12:15–20.

Joyner AL, Herrup K, Auerbach BA, Davis CA, Rossant J (1991) Subtle cerebellar phenotype in mice homozygous for a targeted deletion of the En-2 homeobox. Science 251:1239–1243.

Jovanovic J, Benfenati F, Siow Y, Sihra T, Sanghera J, Pelech S, Greengard P, Czernik A (1996) Neurotrophins stimulate phosphorylation of synapsin I by MAP kinase and regulate synapsin I-actin interactions. Proc Natl Acad Sci USA 93:3679–3683.

Kuemerle B, Zanjani H, Joyner A, Herrup K (1997) Pattern deformities and cell loss in Engrailed-2 mutant mice suggest two separate patterning events during cerebellar development. J Neurosci 17:7881–7889.

Kushner SA, Elgersma Y, Murphy GG, Jaarsma D, van Woerden GM, Hojjati MR, Cui Y, LeBoutillier JC, Marrone DF, Choi ES, De Zeeuw CI, Petit TL, Pozzo-Miller L, Silva AJ (2005) Modulation of presynaptic plasticity and learning by the H-ras/extracellular signal-regulated kinase/synapsin I signaling pathway. J Neurosci 25:9721–9734.

Lin YL, Hsueh YP (2008) Neurofibromin interacts with CRMP-2 and CRMP-4 in rat brain. Biochem Biophys Res Commun 369:747–752.

Matsubara M, Kusubata M, Ishiguro K, Uchida T, Titani K, Taniguchi H (1996) Site-specific phosphorylation of synapsin I by mitogen-activated protein kinase and Cdk5 and its effects on physiological functions. J Biol Chem 271:21108–21113.

Meng X, Peng B, Shi J, Zheng Y, Chen H, Zhang J, Li L, Zhang C (2006) Effects of overexpression of Sim2 on spatial memory and expression of synapsin I in rat hippocampus. Cell Biol Int 30:841–847.

Molteni R, Wu A, Vaynman S, Ying Z, Barnard RJ, Gómez-Pinilla F (2004) Exercise reverses the harmful effects of consumption of a high-fat diet on synaptic and behavioral plasticity associated to the action of brain-derived neurotrophic factor. Neuroscience 123:429–440.

Nayak AS, Moore CI, Browning MD (1996) Ca2 + /calmodulin-dependent protein kinase II phosphorylation of the presynaptic protein synapsin I is persistently increased during long-term potentiation. Proc Natl Acad Sci USA 93:15451–15456.

Nowicka D, Liguz-Lecznar M, Skangiel-Kramska J (2003) A surface antigen delineating a subset of neurons in the primary somatosensory cortex of the mouse. Acta Neurobiol Exp 63:185–195.

Patrakitkomjorn S, Kobayashi D, Morikawa T, Wilson MM, Tsubota N, Irie A, Ozawa T, Aoki M, Arimura N, Kaibuchi K, Saya H, Araki N (2008) Neurofibromatosis type 1 (NF1) tumor suppressor, neurofibromin, regulates the neuronal differentiation of PC12 cells via its associating protein, CRMP-2. J Biol Chem 283:9399–9413.

Provenzano G, Pangrazzi L, Poli A, Pernigo M, Sgadò P, Genovesi S, Zunino G, Berardi N, Casarosa S, Bozzi Y (2014) Hippocampal dysregulation of neurofibromin-dependent pathways is associated with impaired spatial learning in Engrailed 2 knockout mice. J Neurosci 34:13281–13288.

Resende LS, Ribeiro AM, Werner D, Hall JM, Savage LM (2012) Thiamine deficiency degrades the link between spatial behavior and hippocampal synapsin I and phosphorylated synapsin I protein levels. Behav Brain Res 232:421–425.

Sgadò P, Genovesi S, Kalinovsky A, Zunino G, Macchi F, Allegra M, Murenu E, Provenzano G, Tripathi PP, Casarosa S, Joyner AL, Bozzi Y (2013a) Loss of GABAergic neurons in the hippocampus and cerebral cortex of Engrailed-2 null mutant mice: implications for autism spectrum disorders. Exp Neurol 247:496–505.

Sgadò P, Provenzano G, Dassi E, Adami V, Zunino G, Genovesi S, Casarosa S, Bozzi Y (2013b) Transcriptome profiling in Engrailed2 knockout mice reveals common molecular pathways associated with ASD. Mol Autism 4:51. http://dx.doi.org/10.1186/2040-2392-4-51.

Sihra TS, Wang JK, Gorelick FS, Greengard P (1989) Translocation of synapsin I in response to depolarization of isolated nerve terminals. Proc Natl Acad Sci U S A 86:8108–8112.

Tripathi PP, Sgadò P, Scali M, Viaggi C, Casarosa S, Simon H, Vaglini F, Corsini GU, Bozzi Y (2009) Increased susceptibility to kainic acid-induced seizures in Engrailed-2 knockout mice. Neuroscience 159:842–849.

(Accepted 13 November 2014)
(Available online 26 November 2014)